Euro. Jnl of Applied Mathematics (2015), *vol.* 26, *pp.* 453–475. © Cambridge University Press 2015
doi:10.1017/S0956792515000145

A Stefan model for mass transfer in a rotating disk reaction vessel

C. S. BOHUN

University of Ontario Institute of Technology, Oshawa, ON L1H 7K4, Canada
email: *sean.bohun@uoit.ca*

(*Received 24 May 2013; revised 26 March 2015; accepted 31 March 2015; first published online 4 May 2015*)

In this paper, we focus on the process of mass transfer in the rotating disk apparatus formulated as a Stefan problem with consideration given to both the hydrodynamics of the process and the specific chemical reactions occurring in the bulk. The wide range in the reaction rates of the underlying chemistry allows for a natural decoupling of the problem into a simplified set of weakly coupled convective–reaction–diffusion equations for the slowly reacting chemical species and a set of algebraic relations for the species that react rapidly. An analysis of the chemical equilibrium conditions identifies an expansion parameter and a reduced model that remains valid for arbitrarily large times. Numerical solutions of the model are compared to an asymptotic analysis revealing three distinct time scales and chemical diffusion boundary layer that lies completely inside the hydrodynamic layer. Formulated as a Stefan problem, the model generalizes the work of Levich (Levich and Spalding (1962) Physicochemical hydrodynamics, vol. 689, Prentice-Hall Englewood Cliffs, NJ) and will help better understand the natural limitations of the rotating disk reaction vessel when consideration is made for the reacting chemical species.

Key words: 97M10; 80A22; 74N25; 92E20; 35B40

1 Introduction

For the many petroleum reserves that are found in sandstone, they are typically extracted through a process of matrix acidization whereby acid is injected into the pores of the formation. The remaining reserves are found in limestone and dolomite formations and are typically fracture acidized. In this latter technique, an acid mixture is injected into the wellbore under high pressure creating fractures that are subsequently etched by the acid to increase the permeability of the formation [21]. Within these structures there can exist a very rich family of anhydrous carbonate species including calcite and aragonite, both with the $CaCO_3$ stoichiometry, but with different crystalline structures. Other mineralized compounds such as dolomite $CaMg(CO_3)_2$ and ankerite $CaFe(CO_3)_2$ are also common, depending on the specific formation.

A convenient way to study these materials when they are brought into contact with an acid is the rotating disk method. With this technique, a disk of the material to be analysed is rotated as it is brought into contact with an acid solvent. The rotating disk induces an

https://doi.org/10.1017/S0956792515000145 Published online by Cambridge University Press

axial flow on the solvent that fans out over the surface of the disk with a boundary layer thickness that is independent of the disk radius and controlled by varying the rate of rotation. The theory, developed initially by Levich [17], has been applied in a variety of situations with varying degrees of success [3, 16, 30], and allows for the determination of the reaction rate, the diffusion coefficient associated with the dissolution and the order of the reaction [8, 21, 22, 30]. Boomer *et al.* [4] provides a classical review of the experimental use of this device.

A challenge of the rotating disk method when applied to reservoir rocks is the significant variability in the acid reaction rate. Taylor and Nasr-El-Din [32] attribute this, in the context of oil reservoir samples, to a wide variation in experimental procedure, and identify a variety of possible factors including: (i) changes in surface area as the sample dissolves; (ii) porosity violating the assumption of a laminar flow on the surface of the stone; and (iii) impurities including clays and acidizing additives. In this paper, we develop a new model for mass transfer in the rotating disk apparatus formulated as a Stefan problem for the dissolution of calcium carbonate as an exemplar of the technique. Calcite (calcium carbonate) is chosen as the reacting material because it plays a central role in reservoirs, being mineralized as limestone, acting as a common cement for sandstone, and its relative abundance in sedimentary formations. It also couples with dissolved carbon dioxide through the formation of carbonic acid which has a global impact effecting acidification of the oceans, degradation of monuments, dissolution of coral reefs and formation of caves and karst landscapes[1]. A review of calcium carbonate focussing on its formation and dissolution can be found in Morse *et al.* [25].

The paper begins with a discussion in Section 2 of the chemistry and the underlying mathematics of the carbonic acid system and how it behaves in the presence of calcium. In Section 3, a Stefan model of dissolution is presented with a von Kármán fluid flow structure where the chemical species are grouped according to how rapidly they react. Justification of using a von Kármán similarity solution for the flow field can be found in Appendix B. Section 4 details the equilibrium states of the chemical system in two distinguished limits. Namely, without the presence of calcium and when calcium has reached the saturation level. A more detailed analysis is deferred to Appendix A. This analysis provides a natural expansion parameter which is developed and explored in Section 5, in the limit of high acidification commensurate with what is used experimentally. Finally in Section 6, the dominant model in the highly acid limit is analysed, asymptotic behaviour extracted and the inherent limitations of determining a reaction order are discussed. Section 7 summarizes the conclusions.

This paper will assume a pure calcite sample and use the full chemical kinetics to help emphasize both the limitations of the underlying model and highlight the sensitivity the rotating disk method with respect to the model parameters. The acidity of the solution will be modified with the addition of hydrochloric acid to the reacting chemical system and to include this possibility, a chlorine ion concentration[2] of $[\mathrm{Cl}^-]$ is also included in the

[1] Karst landscapes are characterized by bedrock laden with carbonate rich minerals that are easily dissolved, forming fissures, sinkholes, caves and underground streams in their wake.

[2] The addition of Cl^- ions corresponds to adding HCl which is assumed to completely disassociate.

https://doi.org/10.1017/S0956792515000145 Published online by Cambridge University Press

model. Initially no Ca^{2+} will be in solution and as the $CaCO_3(s)$ dissolves, $[Ca^{2+}]$ increases asymptotically approaching its solubility limit at large times. As well, the chemical species are assumed to be at equilibrium at both the dissolving interface and far into the bulk at a specified inflow boundary. An axisymmetric model is chosen for simplicity despite the existence of piping with the experimental apparatus for sampling and draining the reactant that may break this symmetry. Commensurate with this, the fluid velocity is assumed to take on a von Kármán similarity solution.

2 The carbonic acid system

In the basic carbonic acid system, carbon dioxide gas, $CO_2(g)$, dissolves in water to its aqueous form and the subsequent formation of carbonic acid, H_2CO_3. The carbonic acid can then decompose into bicarbonate HCO_3^- and carbonate CO_3^{2-} ions, depending upon the $pH = -\log_{10}[H^+]$ of the solution. The square bracket notation $[A]$ denotes the concentration of species A and for this paper, concentration is measured in units of moles of material per litre of solution, denoted as M. The system of reactions can be summarized as follows:

$$CO_2(g) \overset{K_H}{\longleftrightarrow} CO_2, \tag{2.1a}$$

$$CO_2 + H_2O \underset{k_{-1}}{\overset{k_1}{\rightleftharpoons}} H_2CO_3^0 \overset{K_1}{\longleftrightarrow} H^+ + HCO_3^-, \tag{2.1b}$$

$$CO_2 + OH^- \underset{k_{-2}}{\overset{k_2}{\rightleftharpoons}} HCO_3^-, \tag{2.1c}$$

$$HCO_3^- \overset{K_2}{\longleftrightarrow} H^+ + CO_3^{2-}, \tag{2.1d}$$

$$H_2O \overset{K_W}{\longleftrightarrow} H^+ + OH^-, \tag{2.1e}$$

where the slower reactions are characterized by rate constants (lowercase) and the fast reactions are given equilibrium constants (uppercase). The superscript '0' on $H_2CO_3^0$ refers to carbonic acid in equilibrium with both the bicarbonate ion and the aqueous carbon dioxide and will be clarified below. In reaction equation (2.1a), $CO_2(g)$ is dissolved and either forms bicarbonate ions directly through equation (2.1c) or is effectively catalysed through the formation of carbonic acid in equation (2.1b). Bicarbonate ions can then disassociate to form carbonate ions in equation (2.1d). The final reaction equation (2.1e) is the equilibrium of water with hydrogen and hydroxide ions. If calcite is present then there is an additional reaction

$$CaCO_3(s) \overset{K_{sp}}{\longleftrightarrow} Ca^{2+} + CO_3^{2-}, \tag{2.1f}$$

which illustrates that as $CaCO_3(s)$ is dissolved by equation (2.1f), the calcium ions that are injected into the solution are influenced by the carbonate ions already present.

A closely related system that neglects equations (2.1c) and (2.1e) is studied in [24] with respect to ocean acidification and it is shown that despite the seeming complexity of the system, there is a natural decoupling of time scales due to the rate coefficients differing by many orders of magnitude. All of the rate and equilibrium constants are temperature

https://doi.org/10.1017/S0956792515000145 Published online by Cambridge University Press

Table 1. *Rate and equilibrium constants associated with the carbonic acid system and the dissolution of calcium carbonate*

Q	Units	$Q(T = 298.15\ \mathrm{K})$	Ref.
k_1	s^{-1}	2.62×10^{-2}	[34]
k_{-1}	s^{-1}	2.67×10^{1}	[34]
k_2	$M^{-1}s^{-1}$	8.42×10^{3}	[34]
k_{-2}	s^{-1}	1.94×10^{-4}	[34]
K_1	M	4.50×10^{-4}	...
K_2	M	4.68×10^{-11}	[29]
K_W	M^2	1.01×10^{-14}	[9]
K_H	$M\ atm^{-1}$	3.40×10^{-2}	[29]
K_{sp}	M^2	4.47×10^{-9}	[27]

dependent but for the purposes of this work, only their values at 25 °C are used and can be found in Table 1.

At high solute concentrations, typical of the acidization process, ion complexes form between the dissolved molecules and ions in solution which inhibit the dissolved species from participating in the thermodynamic equilibrium. The consequence of this is that the equilibrium constants depend not only on the temperature but also on the ionic environment, characterized by the ionic strength of the solution

$$I = \frac{1}{2}\sum_i [\mathsf{A}_i] q_i^2, \tag{2.2}$$

where q_i denotes the electric charge of species A_i, and the sum is taken over all of the ion species. To model these Coulombic interactions between ions one defines the activity of a compound A, denoted by (A), as $(\mathsf{A}) = \gamma_{\mathsf{A}}[\mathsf{A}]$ where $\gamma_{\mathsf{A}} = \gamma_{\mathsf{A}}(I)$, known as the activity coefficient of A, is a function of the ionic strength of the solution. In the thermodynamic equilibrium, concentrations should be replaced by the activity.

As mentioned earlier, $\mathsf{H_2CO_3^0}$ refers to the carbonic acid that is in simultaneous equilibrium with the dissolved carbon dioxide and the bicarbonate ion. Because of this, the equilibrium coefficient K_1 can be calculated from the other rate constants and two values are often quoted in the literature: a true ionization constant and an apparent equilibrium constant. If equations (2.1b), (2.1c) and (2.1e) are in equilibrium then

$$k_1(\mathsf{CO_2}) = k_{-1}(\mathsf{H_2CO_3^0}), \qquad k_2(\mathsf{CO_2})(\mathsf{OH^-}) = k_{-2}(\mathsf{HCO_3^-}), \qquad K_W = (\mathsf{H^+})(\mathsf{OH^-}). \tag{2.3}$$

Combining these gives the true ionization constant of $\mathsf{H_2CO_3^0}$

$$K_1 = \frac{(\mathsf{H^+})(\mathsf{HCO_3^-})}{(\mathsf{H_2CO_3^0})} = \frac{k_{-1}k_2}{k_1k_{-2}}K_W \sim 4.49 \times 10^{-4}. \tag{2.4}$$

The apparent equilibrium constant, due to most of the carbonic acid converting into

https://doi.org/10.1017/S0956792515000145 Published online by Cambridge University Press

aqueous carbon dioxide, is[3]

$$K_1' = \frac{(\mathrm{H}^+)(\mathrm{HCO}_3^-)}{(\mathrm{CO}_2 + \mathrm{H}_2\mathrm{CO}_3^0)} = \frac{k_1}{k_1 + k_{-1}} K_1 \sim 4.40 \times 10^{-7}. \tag{2.5}$$

Even though the large variation in the equilibrium constants dominates the chemical behaviour of the carbonate system, various models can be found in the literature that include this effect. The extended Debye–Hückel model used in Kaufmann *et al.* [11] accounts for the differing ion sizes, yet is applicable at only moderate ionic strengths ($I < 10^{-1}$ M). At higher levels (10^{-1} M $< I <$ 0.5 M) other models exist (Davies [6], Pitzer & Brewer [18, 28]). Common to all of these models is the general form

$$\log_{10} \gamma_q = q^2 G(I), \qquad G(0) = 0, \tag{2.6}$$

quadratic in the charge for some continuous function G that depends primarily on the ionic strength of the solution with $\gamma_q \to 1$ as $I \to 0$. Rather than using activities, we can convert to concentrations using the activity coefficients and then absorb them into a compensated equilibrium constant. For the specific reactions in this paper, using $\gamma_0 = 1$, and $\gamma_2 = \gamma_1^4$ from the form of equation (2.6), gives

$$K_1^c = \frac{K_1}{\gamma_1^2} = \frac{[\mathrm{H}^+][\mathrm{HCO}_3^-]}{[\mathrm{H}_2\mathrm{CO}_3^0]}, \quad K_2^c = \frac{K_2}{\gamma_1^4} = \frac{[\mathrm{H}^+][\mathrm{CO}_3^{2-}]}{[\mathrm{HCO}_3^-]}, \quad K_{\mathrm{W}}^c = \frac{K_{\mathrm{W}}}{\gamma_1^2} = [\mathrm{H}^+][\mathrm{OH}^-], \tag{2.7}$$

where γ_1 is determined experimentally. In the absence of this experimental data, and since this is a secondary effect when compared to the variation of the equilibrium values over many orders of magnitude in this chemical system, a value of $\gamma_1 = 1$ is used in all of the numerical solutions yet the notation for compensated equilibrium constants is used throughout to denote this effect.

3 The model

For this system there is a natural decoupling of the chemistry into chemical species that evolve rapidly and those that evolve slowly. Those that evolve rapidly are prescribed by the equilibrium relations set up in the previous section, whereas the slowly varying species satisfy convective–reaction–diffusion equations.

Figure 1 illustrates the main features of the domain under consideration. A sample of $\mathrm{CaCO}_3(\mathrm{s})$ spinning at a constant angular rate ω and undergoing dissolution at $z = S(t)$, the products of which are transported into the bulk. The domain of consideration Ω is bounded by the free boundary of the dissolving sample Γ_S, an inflow boundary Γ_∞ where well-mixed fluid enters and an outflow boundary Γ_R so that there is no net fluid flow through the closed boundary $\partial\Omega = \Gamma_S \cup \Gamma_\infty \cup \Gamma_R$. The various physical parameters for this process are collected into Table 2.

[3] See Kern [12] for more details.

https://doi.org/10.1017/S0956792515000145 Published online by Cambridge University Press

Table 2. *Remaining physical parameters for the dissolution process*

Data	Symbol	Units	Value	Ref.
Diffusion coefficient of CO_2	$D_{[CO_2]}$	m^2s^{-1}	2.07×10^{-9}	[37]
Diffusion coefficient of H^+	$D_{[H^+]}$	m^2s^{-1}	9.31×10^{-9}	[35]
Diffusion coefficient of Cl^-	$D_{[Cl^-]}$	m^2s^{-1}	2.03×10^{-9}	[35]
Diffusion coefficient of Ca^{2+}	$D_{[Ca^{2+}]}$	m^2s^{-1}	0.793×10^{-9}	[35]
Kinetic viscosity of water	ν	m^2s^{-1}	9.82×10^{-7}	[13]
Calcium concentration within calcite	c_s	M	27.1	[27]
$CO_2(g)$ partial pressure in air at 1 atm	$P_{CO_2(g)}$	atm	3.5×10^{-4}	...
Nominal air pressure	...	atm	55	[1]
Nominal rotation rate	ω	rpm	100	[1]
Nominal $[Cl^-]$	...	M	4.4	[1]
Area of sample	πR_d^2	m^2	1.15×10^{-3}	[1]
Volume of reaction vessel	$\pi R_v^2 H_v$	m^3	10^{-3}	[1]

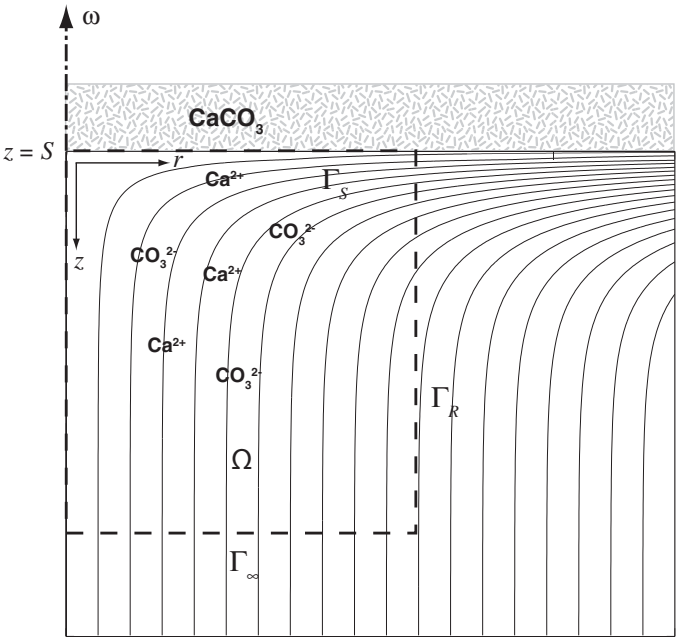


FIGURE 1. General features of the domain for the model within the rotating disk apparatus. A sample of calcite, $CaCO_3(s)$, spins at a constant rotation rate of ω and material dissolves into solution at $z = S$. Due to the rotation the fluid wells up from the bottom of the reaction vessel and then fans out over the surface of the reacting sample.

Within the bulk of the domain Ω, the concentration of the slowly evolving species $\{CO_2, HCO_3^-, Ca^{2+}\}$ satisfy a system of convective–reaction–diffusion equations

$$\frac{\partial U_i}{\partial t} + \mathbf{v} \circ \nabla U_i - D_i \nabla^2 U_i = R_i, \qquad \mathbf{x} \in \Omega, \quad t > 0, \tag{3.1a}$$

https://doi.org/10.1017/S0956792515000145 Published online by Cambridge University Press

where $U = ([CO_2], [HCO_3^-], [Ca^{2+}])$, $D = (D_{[CO_2]}, D_{\text{eff}}, D_{\text{eff}})$ and $R = (\mathscr{R}, -\mathscr{R}, 0)$ with the reaction term

$$\mathscr{R} = -k_1[CO_2] + \frac{k_{-1}}{K_1^c}[H^+][HCO_3^-] - k_2 K_W^c \frac{[CO_2]}{[H^+]} + k_{-2}[HCO_3^-], \tag{3.1b}$$

determined by equations (2.1b), (2.1c) and (2.7). The fluid velocity $\mathbf{v}$ satisfies the Navier–Stokes equations and are omitted at this point simply for brevity. The effective diffusion coefficient for the charged species is estimated by the Nernst–Hartley relation [14]

$$D_{\text{eff}} = \frac{(q_+ + |q_-|)\, D_+ D_-}{q_+ D_+ + |q_-| D_-}, \tag{3.1c}$$

where the ionic environment is characterized by a single dominant cation–anion pair with respective charges (q_+, q_-) and diffusion coefficients (D_+, D_-). The rapidly evolving species $\{H_2CO_3^0,\ OH^-,\ CO_3^{2-}\}$ are determined from the slower reactions through the equilibrium condition (2.7)

$$[H_2CO_3^0] = \frac{[H^+][HCO_3^-]}{K_1^c}, \qquad [OH^-] = \frac{K_W^c}{[H^+]}, \qquad [CO_3^{2-}] = \frac{K_2^c[HCO_3^-]}{[H^+]}, \tag{3.1d}$$

and the system is closed with a condition of charge neutrality

$$[H^+] + 2[Ca^{2+}] - [OH^-] - [HCO_3^-] - 2[CO_3^{2-}] - [Cl^-] = 0, \tag{3.1e}$$

where $[Cl^-]$ is set externally to specify the initial acidity of the solvent.

The dissolution interface is denoted by Γ_S and is given explicitly by

$$z - S(\mathbf{x}, t) = 0, \qquad \mathbf{x} \in \Gamma_S. \tag{3.2}$$

At this interface the concentration of calcium reaches its solubility limit and the other chemical species are chosen to be consistent with this equilibrium state. Consequently, the concentration of bicarbonate is chosen to be consistent with this equilibrium and since no carbon dioxide is produced at this interface, the diffusive flux of the dissolved carbon dioxide vanishes, giving the conditions

$$\frac{\partial}{\partial \mathbf{n}}[CO_2] = 0, \qquad [HCO_3^-] = \frac{K_1^c[H_2CO_3^0]}{[H^+]}, \qquad [Ca^{2+}] = [Ca^{2+}]_{\max}, \qquad \mathbf{x} \in \Gamma_S. \tag{3.3}$$

The motion of the dissolution interface is governed by the Stefan condition

$$\left(c_s - [Ca^{2+}]\right) \mathbf{v}_n \circ \mathbf{n} = -D_{\text{eff}} \frac{\partial}{\partial \mathbf{n}}[Ca^{2+}], \qquad \mathbf{x} \in \Gamma_S, \tag{3.4a}$$

where c_s is the concentration of the undissolved calcium bound in the calcite crystalline lattice and $\mathbf{v}_n = v_n \mathbf{n}$ is the speed at which the interface moves in the direction of its outward unit normal $\mathbf{n}$. If $\partial S/\partial t$ denotes the speed of the interface in the $\mathbf{k}$ direction, then

$$\mathbf{v}_n \circ \mathbf{n} = v_n = \frac{\partial S}{\partial t} \mathbf{k} \circ \mathbf{n}. \tag{3.4b}$$

https://doi.org/10.1017/S0956792515000145 Published online by Cambridge University Press

Away from the dissolving interface we denote an inflow boundary Γ_∞ where the chemical species are in equilibrium and the dissolved CO_2 is governed by the external partial pressure of $CO_2(g)$, so that

$$[CO_2] = K_H P_{CO_2(g)}, \qquad [HCO_3^-] = \frac{K_1^c [H_2CO_3^0]}{[H^+]}, \qquad \mathbf{x} \in \Gamma_\infty. \tag{3.5}$$

For the calcium ions, if the system was open then one could apply a no flux condition, but since the system is closed, the amount of dissolved calcite should reflect the concentration of calcium far from the interface. Assuming a well-mixed chemical solution, variations in $[Ca^{2+}]$ only in the axial direction and no change in the solution volume during dissolution gives the condition

$$\pi R_d^2 \, |S(t)| \, c_s = \pi R_v^2 H_v [Ca^{2+}], \qquad \mathbf{x} \in \Gamma_\infty, \tag{3.6}$$

correct up to a factor dependent on the ratio boundary layer thickness to the vessel height and the ratio of the calcium concentrations at the dissolution interface and the far-field.

One of the inherent challenges of the carbonic acid/calcite system is the variation of the behaviour with the acidity. To find an effective scale each of the chemical species we begin by determining the equilibrium states of equation (2.1) in two limiting regimes: (i) when no calcium is present and (ii) when the calcium concentration has reached its solubility limit. This procedure systematically connects the chemical behaviour at the dissolution interface with the chemistry in the bulk of the reaction vessel, as well as providing a natural hierarchy of the various chemical effects.

4 Equilibrium conditions

When the experiment commences there is initially no dissolved calcium and as the experiment progresses, this level increases until it eventually reaches a maximum governed by the solubility product K_{sp} that satisfies the inequality

$$K_{sp} \geqslant [Ca^{2+}][CO_3^{2-}]. \tag{4.1}$$

If all of the chemical constituents are in equilibrium, then along with equations (3.1d) and (3.1e), we also have, from equations (2.1a) and (2.1b), the equalities

$$[CO_2] = K_H P_{CO_2(g)}, \qquad k_1 [CO_2] = k_{-1} [H_2CO_3^0]. \tag{4.2}$$

Combining all of the equilibrium conditions into equation (3.1e) gives the algebraic expression

$$2 \min \left([Ca^{2+}]_{max}, [Ca^{2+}] \right) [H^+]^2 + [H^+]^3 - [Cl^-][H^+]^2 - \left(K_W^c + K_P \right) [H^+] - 2K_2^c K_P = 0, \tag{4.3a}$$

where

$$[Ca^{2+}]_{max} = \frac{[H^+]^2}{2\lambda K_P}, \qquad \lambda = \frac{K_2^c}{2K_{sp}}, \qquad K_P = \frac{k_1}{k_{-1}} K_1^c K_H P_{CO_2(g)}. \tag{4.3b}$$

https://doi.org/10.1017/S0956792515000145 Published online by Cambridge University Press

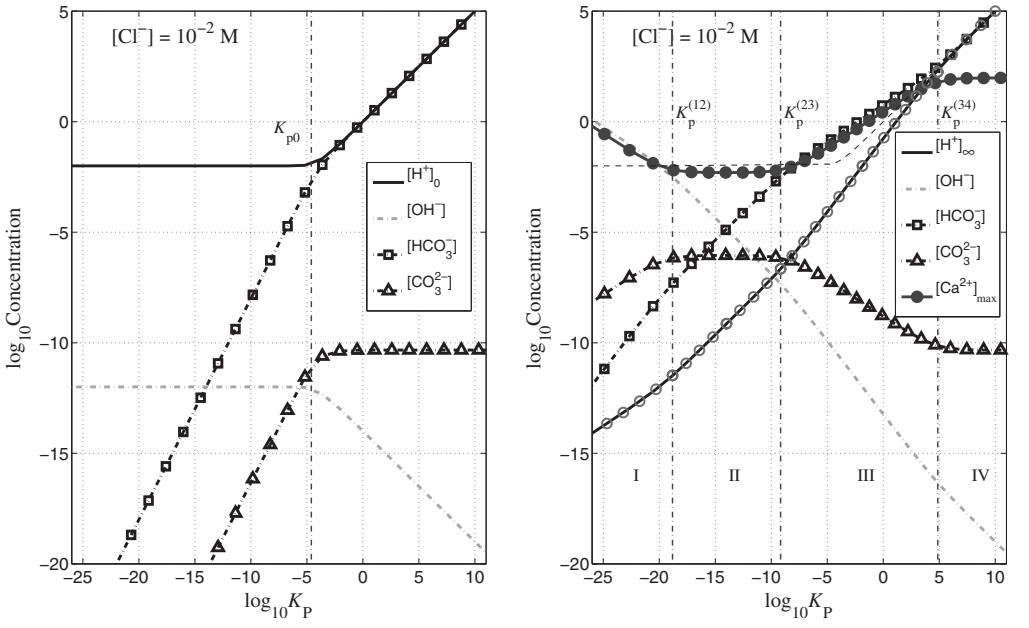


FIGURE 2. Effect of carbon dioxide partial pressure on the equilibrium concentration of the various ionic species in the carbon dioxide-water system (2.1) for $[\mathrm{Cl}^-] = 10^{-2}$ M. To the left is the case when $[\mathrm{Ca}^{2+}] = 0$ and to the right is the case when $[\mathrm{Ca}^{2+}] = [\mathrm{Ca}^{2+}]_{\max}$. The $[\mathrm{H}^+]_0$ also appears as a dashed line in the right panel for comparison with $[\mathrm{H}^+]_\infty$ and the composite first order expression given by equation (A 3) is indicated by the open circles on the $[\mathrm{H}^+]_\infty$ curve.

For the initial level of hydrogen ion concentration we set $[\mathrm{Ca}^{2+}] = 0$ and consider

$$[\mathrm{H}^+]_0^3 - [\mathrm{Cl}^-][\mathrm{H}^+]_0^2 - \left(K_{\mathrm{W}}^c + K_{\mathrm{P}}\right)[\mathrm{H}^+]_0 - 2K_2^c K_{\mathrm{P}} = 0, \tag{4.4}$$

with $[\cdot]_0$ indicating the absence of calcium. Using the data in Table 1, and for illustrative purposes $[\mathrm{Cl}^-] = 10^{-2}$ M, the left panel of Figure 2 shows the two solution regimes separated by a transition region at $K_{\mathrm{P}}^{1/2} = K_{\mathrm{P0}}^{1/2} = \frac{[\mathrm{Cl}^-]}{2} + (\frac{[\mathrm{Cl}^-]^2}{4} + K_{\mathrm{W}}^c)^{1/2}$. To determine the maximum possible $[\mathrm{Ca}^{2+}]$ we consider

$$\frac{1}{\lambda K_{\mathrm{P}}}[\mathrm{H}^+]_\infty^4 + [\mathrm{H}^+]_\infty^3 - [\mathrm{Cl}^-][\mathrm{H}^+]_\infty^2 - \left(K_{\mathrm{W}}^c + K_{\mathrm{P}}\right)[\mathrm{H}^+]_\infty - 2K_2^c K_{\mathrm{P}} = 0, \tag{4.5}$$

where the notation $[\cdot]_\infty$ indicates that the hydrogen ion concentration corresponds to the terminal condition when the maximum amount of calcium has been dissolved. Although simply an algebraic expression (4.5) belies the richness of the underlying equilibrium chemistry. Analysing equation (4.5) we see that it decouples into four distinct behaviours (to order 0) with respect to K_{P} indicating significant shifts in the chemical landscape. These behaviours are straightforward to extract using a dominant balance technique and are visible in the right panel of Figure 2 which shows the behaviour of all of the ionic species across these four regions for $[\mathrm{Cl}^-] = 10^{-2}$ M. Further analysis of the equilibrium states is deferred to Appendix A.

https://doi.org/10.1017/S0956792515000145 Published online by Cambridge University Press

5 The reduced model

5.1 Non-dimensionalization

To find appropriate scalings for the various chemical species, we appeal to the experimental conditions in Table 2 to find $[\mathrm{H}^+]_0 = 4.4$ M, $[\mathrm{H}^+]_\infty = 2.58 \times 10^{-6}$ M and our expansion parameter is

$$\epsilon = \frac{[\mathrm{H}^+]_\infty}{[\mathrm{H}^+]_0} \simeq 5.86 \times 10^{-7}. \tag{5.1}$$

We seek an asymptotic expansion in terms of ϵ which motivates the following scalings:

$$h = \frac{[\mathrm{H}^+]}{[\mathrm{H}^+]_0}, \qquad u = \frac{[\mathrm{CO}_2]}{K_\mathrm{H} P_{\mathrm{CO}_2(\mathrm{g})}}, \qquad b = \frac{[\mathrm{HCO}_3^-][\mathrm{H}^+]_\infty}{K_\mathrm{P}}, \qquad c = \frac{[\mathrm{Ca}^{2+}]}{[\mathrm{Ca}^{2+}]_{\max}}, \tag{5.2}$$

where the lowercase letters are the non-dimensional quantities.

The assumed a von Kármán similarity solution implies the non-dimensionalization

$$\begin{aligned} z &= (\nu/\omega)^{1/2}\hat{z}, \quad S = (\nu/\omega)^{1/2}\hat{S}, \quad r = R_d\hat{r}, \\ u_r &= r\omega\mathscr{F}(\hat{z}), \quad u_\theta = r\omega\mathscr{G}(\hat{z}), \quad u_z = (\nu\omega)^{1/2}\mathscr{H}(\hat{z}), \end{aligned} \tag{5.3a}$$

where $\mathscr{F}, \mathscr{G}, \mathscr{H}$ are non-dimensional functions of the coordinate $\hat{z}$ and where ν is the kinematic viscosity of the fluid. Near the surface of the dissolving stone the dominant ionic species are Ca^{2+} and Cl^- with $2[\mathrm{Ca}^{2+}] \simeq [\mathrm{Cl}^-]$ and far from the interface $[\mathrm{H}^+] \simeq [\mathrm{Cl}^-]$ so that the effective diffusion constant in these regions is respectively

$$D_{\mathrm{eff},\Gamma_S} = \frac{3D_{[\mathrm{Ca}^{2+}]}D_{[\mathrm{Cl}^-]}}{2D_{[\mathrm{Ca}^{2+}]} + D_{[\mathrm{Cl}^-]}} \simeq 0.645 D_{[\mathrm{CO}_2]}, \quad D_{\mathrm{eff},\Gamma_\infty} = \frac{2D_{[\mathrm{H}^+]}D_{[\mathrm{Cl}^-}}{D_{[\mathrm{H}^+]} + D_{[\mathrm{Cl}^-]}} \simeq 1.61 D_{[\mathrm{CO}_2]}. \tag{5.3b}$$

This shows that there is only a modest variation in the diffusion coefficient and to simplify the analysis we replace D_{eff} with $D_{[\mathrm{CO}_2]}$ in what follows. Finally, we use the Stefan condition (3.4) to determine the time scale since we are primarily interested in the time scale on which dissolution is occurring. This gives

$$t = \frac{\mathrm{St}\,\mathrm{Sc}}{\omega}\hat{t}, \quad \mathrm{St} = \frac{c_s}{[\mathrm{Ca}^{2+}]_{\max}} - 1 \simeq 11.3, \quad \mathrm{Sc} = \frac{\nu}{D_{[\mathrm{CO}_2]}} \simeq 474, \quad \mathrm{Re} = \frac{\omega R_d^2}{\nu} \simeq 2.34 \times 10^5, \tag{5.3c}$$

using the data in Table 2.

The large Stefan number, St, indicates that the dissolution can be treated as quasi-steady, while the large Schmidt number, Sc, implies that there is a mass transfer boundary layer that lies inside the viscous boundary at the dissolution interface. In fact, the product St Sc is a measure of the ratio of the characteristic speed of the fluid moving axially towards the sample and the speed at which that interface dissolves since

$$\frac{\left|\frac{\mathrm{d}S}{\mathrm{d}t}\right|}{|u_z|} = \frac{1}{\mathrm{St}\,\mathrm{Sc}}\frac{1}{\mathscr{H}}\frac{\mathrm{d}\hat{S}}{\mathrm{d}\hat{t}} \simeq 1.87 \times 10^{-4}, \tag{5.4}$$

when the non-dimensional quantities are $\mathscr{O}(1)$.

https://doi.org/10.1017/S0956792515000145 Published online by Cambridge University Press

In terms of these non-dimensional coordinates, and the chosen expansion parameter, the field variables satisfy

$$\begin{aligned}\frac{1}{\mathrm{St}}\frac{\partial \hat{U}_i}{\partial \hat{t}} - \frac{\partial^2 \hat{U}_i}{\partial \hat{z}^2} - \frac{1}{\mathrm{Re}}\frac{1}{\hat{r}}\frac{\partial}{\partial \hat{r}}\left(\hat{r}\frac{\partial \hat{U}_i}{\partial \hat{r}}\right) + \mathrm{Sc}\left(\hat{r}\mathscr{F}\frac{\partial \hat{U}_i}{\partial \hat{r}} + \mathscr{H}\frac{\partial \hat{U}_i}{\partial \hat{z}}\right) \\ = -\frac{k_1}{\omega}\,\mathrm{Sc}\,\hat{G}_i\left(1+\frac{\alpha_0}{h}\epsilon^{3/2}\right)\left(u - \frac{bh}{\epsilon}\right), \qquad \mathbf{x}\in\Omega, \quad t>0,\end{aligned} \tag{5.5a}$$

with $\hat{U}_i = (u, b, c)$, $\hat{G}_i = (1, -\beta, 0)$ and

$$\beta^{-1} = \frac{1}{K_{\mathrm{H}} P_{\mathrm{CO_2(g)}}}\frac{K_{\mathrm{P}}}{[\mathrm{H}^+]_\infty} \simeq 0.171. \tag{5.5b}$$

Similarly, the condition of charge neutrality (3.1e) becomes

$$h^2 + (\alpha_1 c - \alpha_2 - \alpha_3 b\epsilon)\,h - \alpha_4(1+\alpha_5 b)\epsilon^{5/2} = 0, \tag{5.5c}$$

using the expansion parameter ϵ with

$$\begin{aligned}&\alpha_0 = \frac{k_2 K_{\mathrm{W}}^c [\mathrm{H}^+]_0^{1/2}}{k_1 [\mathrm{H}^+]_\infty^{3/2}} \simeq 1.65, \quad \alpha_1 = \frac{[\mathrm{H}^+]_\infty^2}{\lambda K_{\mathrm{P}} [\mathrm{H}^+]_0} \simeq 1.00, \quad \alpha_2 = \frac{[\mathrm{Cl}^-]}{[\mathrm{H}^+]_0} \simeq 1.00, \\ &\alpha_3 = \frac{K_{\mathrm{P}}}{[\mathrm{H}^+]_\infty^2} \simeq 43.4, \qquad \alpha_4 = \frac{K_{\mathrm{W}}^c [\mathrm{H}^+]_0^{1/2}}{[\mathrm{H}^+]_\infty^{5/2}} \simeq 1.99, \quad \alpha_5 = \frac{2K_2^c K_{\mathrm{P}}}{K_{\mathrm{W}}^c [\mathrm{H}^+]_\infty} \simeq 1.03.\end{aligned} \tag{5.5d}$$

The boundary conditions (3.3), (3.5) and (3.6) become

$$\begin{aligned}&\frac{\partial u}{\partial \hat{z}} = \frac{1}{\mathrm{Re}}\frac{\partial \hat{S}}{\partial \hat{r}}\frac{\partial u}{\partial \hat{r}}, \quad b = u, \quad c = 1, && \mathbf{x}\in\Gamma_S, \\ &u = 1, && b = \frac{\epsilon}{h}, \quad c = \frac{\pi R_d^2 \left(\nu/\omega\right)^{1/2}}{\pi R_v^2 H_v}(\mathrm{St}+1)|\hat{S}|, \quad \mathbf{x}\in\Gamma_\infty,\end{aligned} \tag{5.5e}$$

using the chemical equilibrium condition $bh = \epsilon u$. The Stefan condition for the dissolution interface (3.4) reduces to

$$\frac{\partial \hat{S}}{\partial \hat{t}} = \frac{\partial c}{\partial \hat{z}} - \frac{1}{\mathrm{Re}}\frac{\partial \hat{S}}{\partial \hat{r}}\frac{\partial c}{\partial \hat{r}}, \qquad \mathbf{x}\in\Gamma_S. \tag{5.5f}$$

The components of the fluid velocity reduce the Navier–Stokes equations to the classical von Kármán system [2, 26, 31, 36]

$$\frac{\mathrm{d}^2\mathscr{F}}{\mathrm{d}\hat{z}^2} = \mathscr{F}^2 - \mathscr{G}^2 + \mathscr{H}\frac{\mathrm{d}\mathscr{F}}{\mathrm{d}\hat{z}}, \qquad \frac{\mathrm{d}^2\mathscr{G}}{\mathrm{d}\hat{z}^2} = 2\mathscr{F}\mathscr{G} + \mathscr{H}\frac{\mathrm{d}\mathscr{G}}{\mathrm{d}\hat{z}}, \qquad 2\mathscr{F} + \frac{\mathrm{d}\mathscr{H}}{\mathrm{d}\hat{z}} = 0, \tag{5.6a}$$

where the last expression comes from the continuity equation. Applying a no-slip condition

https://doi.org/10.1017/S0956792515000145 Published online by Cambridge University Press

at the dissolution interface and imposing axial flow on the inflow boundary Γ_∞ gives the boundary conditions

$$\mathscr{F}=0, \mathscr{G}=1, \mathscr{H}=0, \quad x\in\Gamma_S, \qquad \mathscr{F}=0, \mathscr{G}=0, \quad x\in\Gamma_\infty. \tag{5.6b}$$

The models (5.5)–(5.6) can be easily modified to reflect either a different flow field or other ranges of acidity by using the analysis in Section 4, and then ultimately through the scaling relationships given by equation (5.5d).

5.2 The zeroth order model

From the form of equation (5.5a) we can now resolve the ϵ dependence of the reaction rate as $\epsilon\to 0$ and to this end, we expand the field variables in the series

$$\begin{pmatrix} u(r,z,t)\\ b(r,z,t)\\ c(r,z,t)\\ S(r,t)\end{pmatrix} = \begin{pmatrix} u_0(z,t)\\ b_0(z,t)\\ c_0(z,t)\\ S(t)\end{pmatrix} + \epsilon^{1/2}\begin{pmatrix} u_1(r,z,t)\\ b_1(r,z,t)\\ c_1(r,z,t)\\ S_1(r,t)\end{pmatrix} + \cdots, \tag{5.7}$$

having dropped the hat notation. Keeping only the zeroth order terms

$$\frac{1}{\mathrm{St}\,\mathrm{Sc}}\frac{\partial u_0}{\partial t} + \mathscr{H}\frac{\partial u_0}{\partial z} - \frac{1}{\mathrm{Sc}}\frac{\partial^2 u_0}{\partial z^2} = -\frac{k_1}{\omega}(u_0-\Gamma_0), \quad \frac{\partial u_0}{\partial z}(S_0,t)=0, \qquad u_0(\infty,t)=1, \tag{5.8a}$$

$$\frac{1}{\mathrm{St}\,\mathrm{Sc}}\frac{\partial b_0}{\partial t} + \mathscr{H}\frac{\partial b_0}{\partial z} - \frac{1}{\mathrm{Sc}}\frac{\partial^2 b_0}{\partial z^2} = \frac{k_1}{\omega}\beta(u_0-\Gamma_0), \quad b_0(S_0,t)=u_0(S_0,t), \quad b_0(\infty,t)=0, \tag{5.8b}$$

$$\frac{1}{\mathrm{St}\,\mathrm{Sc}}\frac{\partial c_0}{\partial t} + \mathscr{H}\frac{\partial c_0}{\partial z} - \frac{1}{\mathrm{Sc}}\frac{\partial^2 c_0}{\partial z^2} = 0, \qquad c_0(S_0,t)=1, \qquad c_0(\infty,t)=\frac{|S_0|}{S_{\max}}, \tag{5.8c}$$

$$\frac{\mathrm{d}S_0}{\mathrm{d}t} = \left.\frac{\partial c_0}{\partial z}\right|_{S_0}, \qquad S_0(0)=0, \tag{5.8d}$$

where

$$\Gamma_0=\max\{b_0, 1-c_0\}, \qquad S_{\max}=\frac{1}{\mathrm{St}+1}\frac{R_v^2 H_v}{R_d^2(v/\omega)^{1/2}} \simeq 1.80\times 10^3, \tag{5.8e}$$

define the reaction term and the maximum possible displacement of the interface.

Returning to dimensional units, $S_{\max}\simeq 7.1$ cm, independent of the rate of rotation, using the data in Table 2. Introducing the moving spatial coordinate $\zeta = z - S_0(t)$ fixes the spatial domain to $\zeta\in[0,\infty)$ but gives an addition term to compensate for this drift.

https://doi.org/10.1017/S0956792515000145 Published online by Cambridge University Press

In detail, expressions (5.8a)–(5.8d) become

$$\mathscr{L}u_0 = -\frac{k_1}{\omega}(u_0 - \Gamma_0), \qquad \frac{\partial u_0}{\partial \zeta}(0,t) = 0, \qquad u_0(\infty,t) = 1, \tag{5.9a}$$

$$\mathscr{L}b_0 = \frac{k_1}{\omega}\beta(u_0 - \Gamma_0), \qquad b_0(0,t) = u_0(0,t), \qquad b_0(\infty,t) = 0, \tag{5.9b}$$

$$\mathscr{L}c_0 = 0, \qquad c_0(0,t) = 1, \qquad c_0(\infty,t) = \frac{|S_0|}{S_{\max}}, \tag{5.9c}$$

$$\frac{\mathrm{d}S_0}{\mathrm{d}t} = \left.\frac{\partial c_0}{\partial \zeta}\right|_{\zeta=0}, \qquad S_0(0) = 0, \tag{5.9d}$$

with

$$\mathscr{L}f = \frac{1}{\mathrm{St}\,\mathrm{Sc}}\left(\frac{\partial f}{\partial t} - S_0'(t)\frac{\partial f}{\partial \zeta}\right) + \mathscr{H}\frac{\partial f}{\partial \zeta} - \frac{1}{\mathrm{Sc}}\frac{\partial^2 f}{\partial \zeta^2}. \tag{5.9e}$$

Similar modifications are made to equation (5.6).

6 Analysis

As we have scaled the z coordinate with $(\nu/\omega)^{1/2}$, the system of equations (5.5)–(5.6), as well as the simplified expressions (5.8), reflect the behaviour in the vicinity of the hydrodynamic boundary layer where the flow moves from predominantly axial to fanning out over the surface of the dissolving sample. The Sc^{-1} factor on the second order terms with the Taylor series for the axial fluid velocity[4], $\mathscr{H}(\eta) = -a\eta^2 + \mathcal{O}(\eta^3)$ with [23] $a = 0.510232$, implies that there is a boundary layer of relative thickness $\mathrm{Sc}^{-1/3} \simeq 0.128$ to the hydrodynamic layer that separates the chemistry at the dissolution interface with chemistry occurring in the bulk.

The quasi-steady state equation ($\mathrm{St} \to \infty$) for the calcium concentration coupled to the Stefan condition becomes

$$\begin{aligned} &\mathscr{H}\frac{\partial c_0^{\mathrm{qs}}}{\partial \zeta} - \frac{1}{\mathrm{Sc}}\frac{\partial^2 c_0^{\mathrm{qs}}}{\partial \zeta^2} = 0, \quad c_0^{\mathrm{qs}}(0,t) = 1, \quad c_0^{\mathrm{qs}}(\infty,t) = \frac{|S_0^{\mathrm{qs}}|}{S_{\max}}, \\ &\frac{\mathrm{d}S_0^{\mathrm{qs}}}{\mathrm{d}t} = \left.\frac{\partial c_0^{\mathrm{qs}}}{\partial \zeta}\right|_{\zeta=0}, \qquad S_0^{\mathrm{qs}}(0) = 0. \end{aligned} \tag{6.1}$$

Solving for c_0^{qs} and then substituting for ζ,

$$c_0^{\mathrm{qs}}(z,t) = 1 + \left(\frac{|S_0^{\mathrm{qs}}(t)|}{S_{\max}} - 1\right)\frac{1}{I_\infty(\mathrm{Sc})}\int_0^{z - S_0^{\mathrm{qs}}(t)} e^{\int^\xi \mathrm{Sc}\,\mathscr{H}(\eta)\,\mathrm{d}\eta}\,\mathrm{d}\xi, \tag{6.2a}$$

where

$$I_\infty(\mathrm{Sc}) = \int_0^\infty e^{\int^\xi \mathrm{Sc}\,\mathscr{H}(\eta)\,\mathrm{d}\eta}\,\mathrm{d}\xi \simeq \left(\frac{a\,\mathrm{Sc}}{3}\right)^{-1/3}\int_0^\infty e^{-\xi^3}\,\mathrm{d}\xi = \left(\frac{a\,\mathrm{Sc}}{3}\right)^{-1/3}\Gamma(4/3), \tag{6.2b}$$

the approximation obtained by only taking the first term in the Taylor series expansion

[4] This particular series is valid when the dissolution interface is stationary.

https://doi.org/10.1017/S0956792515000145 Published online by Cambridge University Press

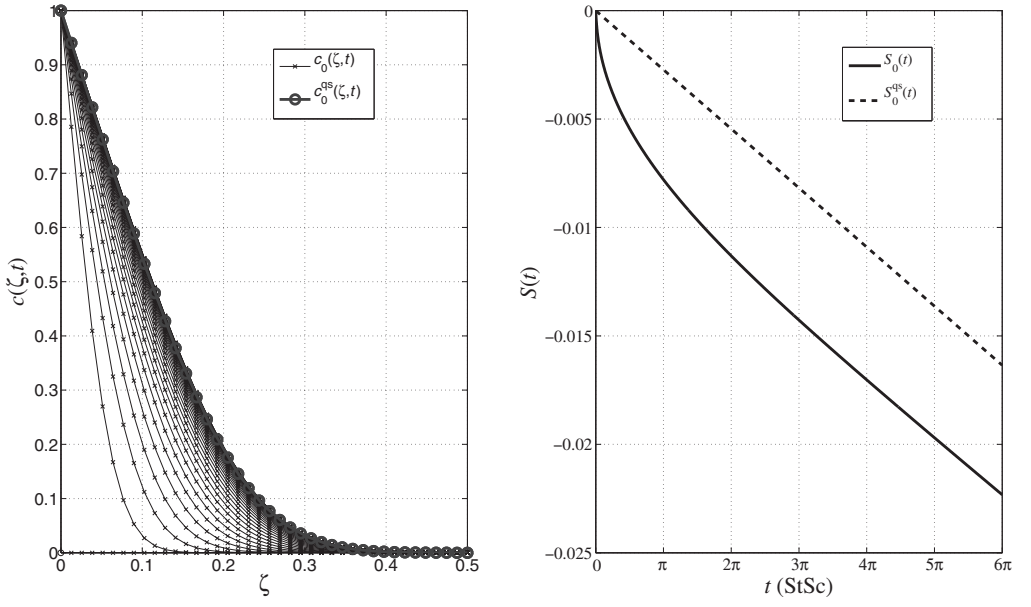


FIGURE 3. Evolution of the fully time dependent calcium concentration $c_0(\zeta,t)$ given by equation (5.8) towards the quasi-steady solution $c_0^{qs}(\zeta,t)$ given by equation (6.4) for $t \in [0, 6\pi(\mathrm{St}\,\mathrm{St})^{-1}]$ corresponding to three rotations. To the right is the corresponding position of the interface in both the unsteady, $S_0(t)$, and quasi-steady $S_0^{qs}(t)$ cases. The nominal experimental air pressure of 55 atm corresponds to $P_{\mathsf{CO}_2(\mathsf{g})} = 1.93 \times 10^{-3}$ atm, and $[\mathsf{Cl}^-] = 4.4$ M.

of $\mathscr{H}$. Using the data in Table 2, $I_\infty(\mathrm{Sc}) = 0.215245$ and the approximation from equation (6.2b) gives $I_\infty(\mathrm{Sc}) \simeq 0.206776$ (4% relative difference).

To complete the calculation we note that the Stefan condition implies that

$$I_\infty(\mathrm{Sc})\frac{\mathrm{d}S_0^{qs}}{\mathrm{d}t} = \frac{\left|S_0^{qs}(t)\right|}{S_{\max}} - 1, \qquad S_0^{qs}(0) = 0, \tag{6.3}$$

so that

$$S_0^{qs}(t) = S_{\max}\left(e^{-t/\tau} - 1\right), \qquad \tau = S_{\max} I_\infty(\mathrm{Sc}), \tag{6.4a}$$

and

$$c_0^{qs}(z,t) = 1 - \frac{e^{-t/\tau}}{I_\infty(\mathrm{Sc})}\int_0^{z-S_0^{qs}(t)} e^{\int^\xi \mathrm{Sc}\,\mathscr{H}(\eta)\,\mathrm{d}\eta}\,\mathrm{d}\xi. \tag{6.4b}$$

Figure 3 shows the time evolution of the $c_0(\zeta,t)$ and $S_0(t)$ satisfying equation (5.8) compared to $c_0^{qs}(\zeta,t)$, $S_0^{qs}(t)$ given by equation (6.4) for $t \in [0, 6\pi(\mathrm{St}\,\mathrm{Sc})^{-1}]$. Dimensionally this corresponds to three full rotations, $t_{\mathrm{dim}} \in [0, 6\pi/\omega]$. After this very short time period the quasi-steady approximation is reached and tracked until the end of the reaction. The large time comparison of the position of the dissolution interface is to the right of Figure 4.

The spatial profiles of u and b do not vary significantly with time and the magnitude of k_1/ω shows that at even slow rates of rotation, the CO_2 and HCO_3^- species are effectively

https://doi.org/10.1017/S0956792515000145 Published online by Cambridge University Press

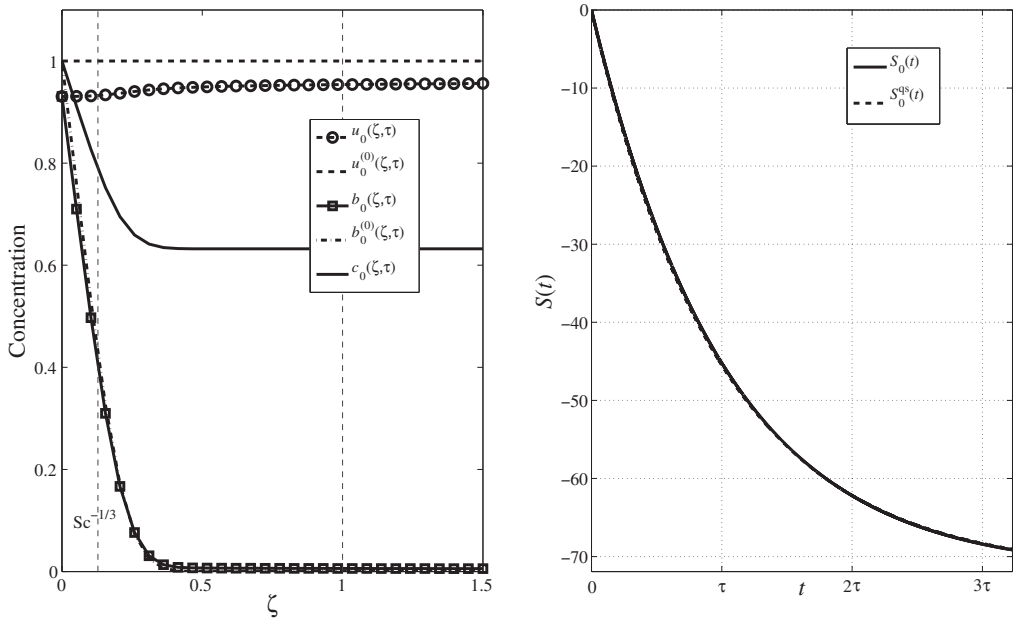


FIGURE 4. To the left are concentration profiles of u_0, b_0, $u_0^{(0)}$, $b_0^{(0)}$ and c_0 at $t = \tau$ for a rotation rate of $\omega = 100$ rpm. In the right panel is behaviour of $S_0(t)$ and $S_0^{\mathrm{qs}}(t)$ for $t \in [0, 3\tau]$ for the same rotation speed.

isolated at this high level of acidity ($\epsilon \sim \mathcal{O}\big([\mathrm{Cl}^-]^{-1/2}\big)$). They are coupled primarily through the boundary conditions rather than the reaction terms. Developing u_0 and b_0 in a series of this quantity,

$$\begin{pmatrix} u_0 \\ b_0 \end{pmatrix} = \begin{pmatrix} u_0^{(0)} \\ b_0^{(0)} \end{pmatrix} + \frac{k_1}{\omega} \begin{pmatrix} u_0^{(1)} \\ b_0^{(1)} \end{pmatrix} + \mathcal{O}\left(\left(\frac{k_1}{\omega} \right)^2 \right), \tag{6.5}$$

shows that

$$u_0^{(0)}(z,t) = 1, \qquad b_0^{(0)}(z,t) = 1 - \frac{1}{I_\infty(\mathrm{Sc})} \int_0^{z-S_0(t)} e^{\int^\xi \mathrm{Sc}\, \mathscr{H}(\eta)\, \mathrm{d}\eta}\, \mathrm{d}\xi, \tag{6.6}$$

with $u_0^{(1)}$, $b_0^{(1)}$ satisfying

$$\begin{gathered} \mathscr{H} \frac{\partial}{\partial z} \begin{pmatrix} u_0^{(1)} \\ b_0^{(1)} \end{pmatrix} - \frac{1}{\mathrm{Sc}} \frac{\partial^2}{\partial z^2} \begin{pmatrix} u_0^{(1)} \\ b_0^{(1)} \end{pmatrix} = \begin{pmatrix} -1 \\ \beta \end{pmatrix} \max\left\{ b_0^{(0)}, 1 - c_0 \right\}, \\ \frac{\partial u_0^{(1)}}{\partial z}(S_0,t) = 0, \quad u_0^{(1)}(\infty,t) = 0, \quad b_0^{(1)}(S_0,t) = u_0^{(1)}(S_0,t), \quad b_0^{(1)}(\infty,t) = 0. \end{gathered} \tag{6.7}$$

Plots of u_0, b_0, $u_0^{(0)}$, $b_0^{(0)}$ and c_0 are collected in Figure 4 over the spatial interval $\zeta \in [0, 1.5]$ at the time $t = \tau = S_{\max} I_\infty(\mathrm{Sc})$. In the right panel of the plot is the time evolution of $S_0(t)$ and $S_0^{\mathrm{qs}}(t)$ for $t \in [0, 3\tau]$, clearly illustrating the exponential decay of the dissolution rate as the calcium reaches its saturation level. Recall that the non-dimensional spatial scales

https://doi.org/10.1017/S0956792515000145 Published online by Cambridge University Press

are in terms of the hydrodynamic boundary layer thickness of $(\nu\omega)^{1/2}$ and that there is a chemical diffusion boundary layer that remains at distance of $\mathrm{Sc}^{-1/3} \simeq 0.128$ from the moving interface. At 100 rpm, the non-dimensional length scale is $(\nu/\omega)^{1/2} = 3.06\times10^{-4}$ m, the time scale is $\mathrm{St}\,\mathrm{Sc}/\omega = 5.11 \times 10^2$ s and $\tau = 50.1$. Consequently, $t = 3\tau$ and $\zeta = 1.5$ respectively correspond to a dimensional time of 21.3 hours and a distance from the dissolution interface of 0.46 mm. By this time the dissolution interface has moved 6.8 cm, about 95% of the maximum possible displacement of 7.1 cm.

6.1 Determining the reaction rate and order

The rotating disk apparatus is used to extract parameters that concern the convection and diffusion of material as it dissolves into the bulk. From the previous analysis, we have seen that there is a thin chemical diffusion boundary layer of roughly $\mathrm{Sc}^{-1/3} \sim 0.128$ of the thickness of the hydrodynamic boundary layer within which the concentration of Ca^{2+} drops from its saturation level, as determined by the initial acidity of the reactant, to a background level, determined by the amount of calcium that has dissolved at any given time. The reaction rate is given by, returning to dimensional coordinates,

$$\begin{aligned} R = -D_{\mathrm{eff}}\,\frac{\partial}{\partial z}[\mathsf{Ca}^{2+}]\bigg|_S &\simeq -D_{[\mathsf{CO}_2]}\left(\frac{\omega}{\nu}\right)^{1/2}\frac{[\mathsf{H}^+]_\infty^2}{2\lambda K_{\mathrm{P}}}\,\frac{\partial c_0}{\partial \hat{z}}\bigg|_{\hat{S}_0} \\ &\simeq D_{[\mathsf{CO}_2]}\left(\frac{\omega}{\nu}\right)^{1/2}\frac{[\mathsf{Cl}^-]}{2}\frac{1}{I_\infty(\mathrm{Sc})}e^{-\hat{t}/\tau} \\ &\simeq \left(\frac{a}{3}\right)^{1/3}\frac{1}{\Gamma(4/3)}D_{[\mathsf{CO}_2]}^{2/3}\nu^{-1/6}\omega^{1/2}\frac{[\mathsf{Cl}^-]}{2}e^{-\hat{t}/\tau}, \end{aligned} \tag{6.8}$$

using the approximation (6.2b). Provided $\hat{t} \ll \tau$, this rate reproduces the result from Levich [17] for a reaction order of $n = 1$. Both the exponential decay with time and the linear relationship between the reaction rate at the surface and the bulk concentration of dissolved calcium have been observed in Kaufmann & Dreybrodt [11] albeit with a different level of acidity and in a different geometry.

By attempting to describe the surface dissolution as a reaction of order n, one is concerned with finding a rate constant k such that

$$R = M(\omega)(1 - c_\infty) = kc_\infty^n, \qquad M(\omega) = \left(\frac{a}{3}\right)^{1/3}\frac{1}{\Gamma(4/3)}D_{\mathrm{eff}}^{2/3}\nu^{-1/6}\omega^{1/2}\frac{[\mathsf{Cl}^-]}{2}, \tag{6.9}$$

where c_∞ denotes the non-dimensional concentration of calcium in the bulk, $c_\infty = c(\infty, t)$. In the case of $n = 1$, one can solve to find that

$$R = \frac{kM(\omega)}{k + M(\omega)} \to \begin{cases} M(\omega), & M(\omega) \ll k \quad \text{(low rotation rates)} \\ k, & M(\omega) \gg k \quad \text{(high rotation rates),} \end{cases} \tag{6.10}$$

implying that the rate is diffusive dominated at low rotation rates with the effective diffusion rate being given by a slope of a plot of reaction rate versus $\omega^{1/2}$. At high rotation rates ($M(\omega) \gg k$) the transport is said to be reaction limited with rate constant k.

https://doi.org/10.1017/S0956792515000145 Published online by Cambridge University Press

Attempting to use this same procedure to determine the order n is problematic since the asymptotic behaviour (equation (6.10)) persists for any order n. This can be seen by considering the perturbative solution of

$$c_\infty^n + \epsilon(c_\infty - 1) = 0, \qquad \epsilon = \frac{M(\omega)}{k}, \tag{6.11a}$$

in the two limits $\epsilon \to 0^+$ and $\epsilon^{-1} \to 0^+$. For low rotation rates ($M(\omega) \ll k$), $c_\infty \sim \epsilon^{1/n} - \frac{1}{n}\epsilon^{2/n} + \mathcal{O}\left(\epsilon^{3/n}\right)$ yielding

$$R = M(\omega)(1 - c_\infty) \sim M(\omega)\left(1 - \epsilon^{1/n} + \mathcal{O}\left(\epsilon^{2/n}\right)\right), \qquad \epsilon \ll 1. \tag{6.11b}$$

For high rotation rates ($M(\omega) \gg k$), $c_\infty \sim 1 - \epsilon^{-1} + n\epsilon^{-2} + \mathcal{O}\left(\epsilon^{-3}\right)$ giving

$$R = M(\omega)(1 - c_\infty) \sim M(\omega)\left(\epsilon^{-1} - n\epsilon^{-2} + \mathcal{O}\left(\epsilon^{-3}\right)\right) = k\left(1 - n\epsilon^{-1} + \mathcal{O}\left(\epsilon^{-2}\right)\right), \quad \epsilon \gg 1. \tag{6.11c}$$

What this illustrates is that even when one is careful to remain in the laminar flow regime first emphasized in the classical work by Levich [17], information about the order of the reaction is naturally suppressed in both the low and high rotation rate limits.

7 Conclusions

A new mathematical model was developed for the dissolution of calcite in a rotating disk apparatus that utilizes the full chemical system and treats the dissolution interface as a free boundary. To develop a model that captures the chemistry over the entire range of possible concentrations, the equilibrium states of the calcium carbonate/carbonic acid system were analysed in detail and a very accurate estimate of the hydrogen concentration was developed for any level of acidity (determined by $[\mathsf{Cl}^-]$) and any partial pressure of $\mathsf{CO}_2(\mathsf{g})$. A natural expansion parameter, in light of this analysis, is the ratio of the hydrogen concentrations that are attainable for the given experimental conditions. This is applied to the special case of the rotating disk apparatus when the reactant is very acidic ($[\mathsf{Cl}^-] = 4.4$ M). To our knowledge neither the asymptotic analysis of the hydrogen concentration nor its utilization to develop an effective expansion parameter for the associated reaction–diffusion–convection equations have appeared in the literature.

Because of the relatively slow reaction rate of aqueous carbon dioxide into carbonic acid compared to the rate of rotation for this apparatus ($k_1/\omega \ll 1$) the evolution of the chemical species and their spatial extent are predominantly governed by the boundary conditions and not the reaction terms. Moving to a higher rotation rate suppresses the reaction terms even further. The large acidity of the initial reactant plays two significant roles. First, it greatly simplifies the dominant chemical processed reflected in a very small expansion parameter ϵ and drives the rate of dissolution. This can be made apparent by briefly returning to dimensional coordinates and noting that

$$\left|\frac{\mathrm{d}S}{\mathrm{d}t}\right| \sim \frac{(\nu\omega)^{1/2}}{\mathrm{St}\,\mathrm{Sc}} \sim \left(\frac{\omega}{\nu}\right)^{1/2} D_{[\mathsf{CO}_2]} \frac{[\mathsf{Cl}^-]/2}{c_s - [\mathsf{Cl}^-]/2}, \tag{7.1}$$

https://doi.org/10.1017/S0956792515000145 Published online by Cambridge University Press

suggesting that in terms of the dissolution rate, a doubling of the initial acid concentration is roughly equivalent to quadrupling the rotational rate.

The analysis also shows that the domain naturally breaks into three spatial regimes and three time intervals. Spatially there is a classical hydrodynamic boundary layer of characteristic thickness $(\nu/\omega)^{1/2}$ where the fluid changes from essentially axial to radial, fanning out over the surface of the dissolving sample. Inside this layer, at relatively one-tenth the thickness, is a chemical diffusion boundary layer that separates the region adjacent to the sample, where the calcium is saturated, to its level in the well-mixed bulk. In summary there is an inner calcium saturated region, a region inside the hydrodynamic layer that is unsaturated and an outer unsaturated region where the fluid flow is effectively axial. With respect to time, there are two characteristic values that break the time evolution into three regimes. For the first few revolutions ($\hat{t} \sim (\mathrm{St}\,\mathrm{Sc})^{-1}$, $t \sim \omega^{-1}$), the boundary and hydrodynamic boundary layers are formed and the dissolution rate established. An effectively constant dissolution rate persists until a time of $\hat{t} = \tau$ ($t = \tau_{\mathrm{dim}}$). Dimensionally, τ_{dim} corresponds to a particular fraction of calcium being dispersed into solution. In particular,

$$M(\omega)\pi R_d^2 \tau_{\mathrm{dim}} = \frac{\mathrm{St}}{\mathrm{St}+1}\frac{[\mathrm{Cl}^-]}{2}\pi R_v^2 H_v. \tag{7.2}$$

Beyond $\hat{t} = \tau$ the reaction begins to slow as one reaches saturation. For $\hat{t}/\tau \ll 1$ the reaction rate predicted by the classical analysis of Levich [17] is recovered in the situation where evolution of the dissolution boundary is governed by a Stefan condition yet caution should be given to extraction of an effective reaction order at the surface. It is shown that examining the reaction rate R as a function of rotation speed ω all lead to the same asymptotic behaviour, independent of the reaction order, in both the low and high rotation limits.

A significant amount of material can be consumed by the reaction for a given geometry and acidity and this can cause problems if the material is not homogeneous. Naturally occurring stone may suffer inclusions and the roughness of the surface would play a role. This can be handled (partially) by updating the flow field, but depending on the nature of the impurities, other chemical reactions may come into play changing the boundary conditions in the bulk and at the surface of the dissolving sample. These particular issues will be raised in a subsequent paper as a further application of the techniques described here. A related problem of slow quiescent flows over rough surfaces is also of considerable interest in both the degradation of man-made structures and cave formation. By looking at a modified fluid flow and comparably low levels of acidity (compared to the situation described here) we hope to extend this method to these other situations. One final issue that will be addressed in a subsequent paper is to determine how well the reaction rate at the surface, as governed by the Stefan relation, compares to the experimentally determined PWP (Plumber, Wigley, Parkhurst) expression that is currently used as an external imposed constraint.

Acknowledgements

The author would like to thank the participants at the First KAUST Study Group on Mathematics for Industry where they were first introduced to this problem. NSERC support from grant RGPIN 341749 is also gratefully acknowledged.

https://doi.org/10.1017/S0956792515000145 Published online by Cambridge University Press

Appendix A Equilibrium analysis of $[H^+]$ with respect to pressure

As stated in Section 4, both $[H^+]_0$ and $[H^+]_\infty$ satisfy algebraic relations that can be solved explicitly for a given set of parameters, but as noticed by Mitchell *et al.* [24], the variability of the parameters over many orders of magnitude decouples the carbonic acid system into effectively disjoint regimes with their accessibility governed by the partial pressure of carbon dioxide and the amount of chlorine in solution. For $[H^+]_0$ this results in the asymptotic expansion

$$[H^+]_0 \sim \begin{cases} K_{P0}^{1/2}\left(1+\frac{1}{2}\frac{1+2\kappa_2}{1-\kappa_1}\left(\frac{K_P}{K_{P0}}\right)+\mathcal{O}\left(\frac{K_P^2}{K_{P0}^2}\right)\right), & K_P \ll K_{P0}, \\ K_P^{1/2}\left(1+(\kappa_1+\kappa_2)\left(\frac{K_{P0}^{1/2}}{K_P^{1/2}}\right)+\mathcal{O}\left(\frac{K_{P0}}{K_P}\right)\right), & K_P \gg K_{P0}, \end{cases} \tag{A 1a}$$

with

$$K_{P0}^{1/2} = \frac{[Cl^-]}{2} + \left(\frac{[Cl^-]^2}{4} + K_W^c\right)^{1/2}, \qquad \kappa_1 = \frac{[Cl^-]}{2K_{P0}^{1/2}}, \qquad \kappa_2 = \frac{K_2^c}{K_{P0}^{1/2}}, \tag{A 1b}$$

so that $0 \leqslant \kappa_1 < \frac{1}{2}$ and using the data in Table 1, $0 < \kappa_2 \leqslant K_2^c {K_W^c}^{-1/2} \sim 4.66 \times 10^{-4}$ as $[Cl^-]$ takes on all possible nonzero values. In the region where[5] $K_P \ll K_{P0}$, $[H^+]_0 \simeq [Cl^-]$ and that the concentration of bicarbonate increases with K_P until $[H^+]_0 \simeq [HCO_3^-]$ for $K_P \gg K_{P0}$.

When calcium is present none of the equilibrium constraints can be neglected. From equation (4.2), at equilibrium, $[CO_2] = \mathcal{O}(K_P)$ and $[H_2CO_3^0] = \mathcal{O}(K_P)$ so if $[H^+] = \mathcal{O}(K_P^s)$ for a given s then[6] from the equilibrium conditions (3.1d), $[HCO_3^-] = \mathcal{O}(K_P^{1-s})$, $[OH^-] = \mathcal{O}(K_P^{-s})$ and $[CO_3^{2-}] = \mathcal{O}(K_P^{1-2s})$ whereas equation (4.3b) implies that $[Ca^{2+}]_{max} = \mathcal{O}(K_P^{2s-1})$.

It is relatively straightforward to show that the solution to show that $[H^+]_\infty$ is monotonic with K_P through differentiation and substitution giving

$$\frac{d[H^+]_\infty}{dK_P} = \frac{\frac{1}{\lambda K_P^2}[H^+]_\infty^4 + [H^+]_\infty + 2K_2^c}{\frac{4}{\lambda K_P}[H^+]_\infty^3 + 3[H^+]_\infty^2 - 2[Cl^-][H^+]_\infty - K_W^c - K_P}, \tag{A 2a}$$

$$= \frac{\left(\frac{1}{\lambda K_P^2}[H^+]_\infty^4 + [H^+]_\infty + 2K_2^c\right)[H^+]_\infty}{\frac{1}{\lambda K_P}[H^+]_\infty^4 + [Cl^-][H^+]_\infty^2 + 2\left(K_W^c + K_P\right)[H^+]_\infty + 6K_2^c K_P} > 0. \tag{A 2b}$$

For small K_P, the dominant *positive* term is $[H^+]_\infty^4/\lambda K_P$, eventually becoming $[H^+]_\infty^3$ as K_P increases. Physically this corresponds to an exchange of the dominant positively charged ionic species from calcium to hydrogen with an increase in partial pressure of carbon dioxide. The dominant *negative* term is more complicated moving from the $K_W^c[H^+]_\infty$ term to $[Cl^-][H^+]_\infty^2$, provided $[Cl^-]$ is large enough, and finally to $K_P[H^+]_\infty$ as K_P increases reflecting exchanges in the dominant negative ionic species from hydroxide to chlorine and finally to bicarbonate ions. A detailed discussion of the equilibrium chemistry can now be revealed.

[5] For very low to vanishing levels of $[Cl^-]$, $[H^+] \simeq [OH^-]$ in the $K_P \ll K_{P0}$ region.

[6] In expressions (A 1), (A 3) and (A 4), $s \in \{0, \frac{1}{2}, \frac{1}{3}, \frac{2}{3}\}$.

https://doi.org/10.1017/S0956792515000145 Published online by Cambridge University Press

Referring to the right panel of Figure 2, in region I K_P is sufficiently small that $[H^+]_\infty^4/\lambda K_P \simeq K_W^c[H^+]_\infty$ corresponding to $2[Ca^{2+}]_{max} \simeq [OH^-]$. In this region, the very low partial pressure drives dissolved CO_2 from solution reducing the amount of HCO_3^- and $H_2CO_3^0$ which in turn drives down $[H^+]$. As $[H^+]_\infty = \mathcal{O}\left(K_P^{1/3}\right)$ in this region, $[HCO_3^-] = \mathcal{O}\left(K_P^{2/3}\right)$ and $[CO_3^{2-}] = \mathcal{O}\left(K_P^{1/3}\right)$ are both increasing and $[Ca^{2+}]_{max} = \mathcal{O}\left(K_P^{-1/3}\right)$, $[OH^-] = \mathcal{O}\left(K_P^{-1/3}\right)$ both decrease with K_P.

For appreciable levels of chlorine, $\lambda[Cl^-]^3 > K_W^c$ ($[Cl^-] \gtrsim 1.25 \times 10^{-4}$ M) the dominant balance becomes $[H^+]_\infty^4/\lambda K_P \simeq [Cl^-][H^+]_\infty^2$ corresponding to $2[Ca^{2+}]_{max} \simeq [Cl^-]$ and indicated as region II on the figure. Because $[OH^-] < [Cl^-] < [HCO_3^-]$, the chlorine ions rather than the hydroxide ions balance the calcium. Noting that from the dominant balance, $[H^+]_\infty = \mathcal{O}\left(K_P^{1/2}\right)$, one has $[HCO_3^-] = \mathcal{O}\left(K_P^{1/2}\right)$, $[OH^-] = \mathcal{O}\left(K_P^{-1/2}\right)$, $[CO_3^{2-}] = \mathcal{O}(1)$ and the maximum amount of dissolved calcium becomes independent of K_P with $[Ca^{2+}]_{max} = \mathcal{O}(1)$.

Increasing K_P further, the bicarbonate level increases until it exceeds $[Cl^-]$ resulting in the formation of region III with a dominant balance of $2[Ca^{2+}]_{max} \simeq [HCO_3^-]$ ($[H^+]_\infty^4/\lambda K_P \simeq K_P[H^+]_\infty$). Because $[H^+]_\infty = \mathcal{O}\left(K_P^{2/3}\right)$, the remaining dependencies are $[HCO_3^-] = \mathcal{O}\left(K_P^{1/3}\right)$, $[OH^-] = \mathcal{O}\left(K_P^{-2/3}\right)$, $[CO_3^{2-}] = \mathcal{O}\left(K_P^{-1/3}\right)$ and $[Ca^{2+}]_{max} = \mathcal{O}\left(K_P^{1/3}\right)$. Finally region IV corresponds to a switch in the dominant positive ionic species to hydrogen ions giving the dominant balance of $[H^+]_\infty^3 \simeq K_P[H^+]_\infty$ yielding $[H^+]_\infty = \mathcal{O}\left(K_P^{1/2}\right)$ as in region II.

For each of these regions one can expand $[H^+]_\infty$ in powers of K_P and build a composite expression for the whole domain. Summarizing the results to the first two nontrivial terms in each branch, when $\lambda[Cl^-]^3 > K_W^c$, gives

$$[H^+]_\infty \sim \begin{cases} [H^+]_{\mathrm{I}} = K_P^{1/3}\left(\left(\lambda K_W^c\right)^{1/3} + \frac{[Cl^-]\lambda^{2/3}}{3K_W^{c\,1/3}}K_P^{1/3}\right), & K_P \ll K_P^{(12)}, \\ [H^+]_{\mathrm{IIa}} = K_P^{1/2}\left(\left(\lambda[Cl^-]\right)^{1/2} + \frac{K_W^c}{2[Cl^-]}K_P^{-1/2}\right), & K_P^{(12)} \ll K_P \ll K_P^{(22)}, \\ [H^+]_{\mathrm{IIb}} = K_P^{1/2}\left(\left(\lambda[Cl^-]\right)^{1/2} + \frac{1}{2[Cl^-]}K_P^{1/2}\right), & K_P^{(22)} \ll K_P \ll K_P^{(23)}, \\ [H^+]_{\mathrm{IIIa}} = K_P^{2/3}\left(\lambda^{1/3} + \frac{[Cl^-]\lambda^{2/3}}{3}K_P^{-1/3}\right), & K_P^{(23)} \ll K_P \ll K_P^{(33)}, \\ [H^+]_{\mathrm{IIIb}} = K_P^{2/3}\left(\lambda^{1/3} - \frac{\lambda}{3}K_P^{1/3}\right), & K_P^{(33)} \ll K_P \ll K_P^{(34)}, \\ [H^+]_{\mathrm{IV}} = K_P^{1/2}\left(1 - \frac{1}{2\lambda}K_P^{-1/2}\right), & K_P \gg K_P^{(34)}, \end{cases} \tag{A 3a}$$

with

$$K_P^{(12)} = \frac{K_W^{c\,2} f^{(12)}}{\lambda[Cl^-]^3}, \quad f^{(12)} \simeq 7.723, \quad K_P^{(22)} = K_W^c,$$

$$K_P^{(23)} = \lambda[Cl^-]^3 f^{(23)}, \quad f^{(23)} \simeq 0.1295, \quad K_P^{(33)} = \frac{[Cl^-]^{3/2}}{\lambda^{1/2}}, \tag{A 3b}$$

$$K_P^{(34)} = \frac{f^{(34)}}{\lambda^2}, \quad f^{(34)} \simeq 2.041,$$

https://doi.org/10.1017/S0956792515000145 Published online by Cambridge University Press

determined by enforcing continuity at the transition points. In detail for $K_{\mathrm{P}}^{(12)}$, matching the lower order terms gives the condition $(\lambda K_{\mathrm{W}}^{c} K_{\mathrm{P}})^{1/3} \simeq (\lambda[\mathsf{Cl}^{-}]K_{\mathrm{P}})^{1/2}$ implying that $K_{\mathrm{P}}^{(12)}$ has the form ${K_{\mathrm{W}}^{c}}^{2}/(\lambda[\mathsf{Cl}^{-}]^{3})$. By letting $K_{\mathrm{P}}^{(12)} = {K_{\mathrm{W}}^{c}}^{2} f^{(12)}/(\lambda[\mathsf{Cl}^{-}]^{3})$ one finds that to enforce continuity at $K_{\mathrm{P}}^{(12)}$, $f^{(12)}$ satisfies $6f^{1/3} + 2f^{2/3} = 6f^{1/2} + 3$ with solution $f^{(12)} \simeq 7.723$. The other values are obtained in a similar fashion and the resulting composite function is displayed in Figure 2.

The effect of changing $[\mathsf{Cl}^{-}]$ only changes the domain of region II and at low enough concentrations, $\lambda[\mathsf{Cl}^{-}]^{3} < K_{\mathrm{W}}^{c}$, branch II is removed and we have the simplified ($[\mathsf{H}^{+}]_{\mathrm{I}}$ and $[\mathsf{H}^{+}]_{\mathrm{IIIa}}$ modified) result

$$[\mathsf{H}^{+}]_{\infty} \sim \begin{cases} [\mathsf{H}^{+}]_{\mathrm{I}} = K_{\mathrm{P}}^{1/3}\left(\left(\lambda K_{\mathrm{W}}^{c}\right)^{1/3} + \frac{\lambda^{1/3}}{3{K_{\mathrm{W}}^{c}}^{2/3}} K_{\mathrm{P}}\right), & K_{\mathrm{P}} \ll K_{\mathrm{W}}^{c}, \\ [\mathsf{H}^{+}]_{\mathrm{IIIa}} = K_{\mathrm{P}}^{2/3}\left(\lambda^{1/3} + \frac{\lambda^{1/3} K_{\mathrm{W}}^{c}}{3} K_{\mathrm{P}}^{-1}\right), & K_{\mathrm{W}}^{c} \ll K_{\mathrm{P}} \ll \frac{{K_{\mathrm{W}}^{c}}^{3/4}}{\lambda^{1/2}}, \\ [\mathsf{H}^{+}]_{\mathrm{IIIb}} = K_{\mathrm{P}}^{2/3}\left(\lambda^{1/3} - \frac{\lambda}{3} K_{\mathrm{P}}^{1/3}\right), & \frac{{K_{\mathrm{W}}^{c}}^{3/4}}{\lambda^{1/2}} \ll K_{\mathrm{P}} \ll K_{\mathrm{P}}^{(34)}, \\ [\mathsf{H}^{+}]_{\mathrm{IV}} = K_{\mathrm{P}}^{1/2}\left(1 - \frac{1}{2\lambda} K_{\mathrm{P}}^{-1/2}\right), & K_{\mathrm{P}} \gg K_{\mathrm{P}}^{(34)}. \end{cases} \tag{A 4}$$

Algebraically, the $[\mathsf{H}^{+}]_{\mathrm{IIIa,b}}$ branches could be lost if region II extended into region IV which would require a chlorine concentration in excess of $\lambda^{-1} \sim 191$ M which is not physically possible.

Appendix B Justification of using von Kármán

The reactant is modelled by the incompressible Navier–Stokes equation and we will argue that, even in the case of a finite radius, a von Kármán similarity solution can be used. This flow field is coupled to a set of convective–reaction–diffusion equations that characterize the slowly evolving chemical constituents which is coupled to a Stefan problem that drives how the dissolution evolves in time.

Consider a cylindrical reaction vessel of radius R_v and height H_v with a rotating disk of radius R_d and angular velocity ω. Tomlan and Hudson [33] used boundary layer analysis on a vorticity formulation to show that when the rotational Reynolds number is large ($\mathrm{Re} = \omega R_d^2/\nu$) and $R_d/R_v \simeq 1$, boundary layers form on all bounding surfaces enclosing an inviscid core. The structure of the flow is similar to that predicted by the von Kármán solution with fluid within the inviscid core moving towards the rotating surface with primarily an axial velocity but having a reduced tangential velocity that is $O(\epsilon^{1/2})$ where $\epsilon = \mathrm{Re}^{-1}$. Reaching the boundary layer of thickness $O(\epsilon^{1/2})$ under the rotating disk, the axial flow reduces to $O(\epsilon^{1/2})$ and both the radial and tangential flows become dominant, fanning the fluid over the surface of the disk towards the side wall to be recirculated. Subsequently, these authors show numerically (validated experimentally in [15]) that for the aspect ratio $R_d = 2H_v$, the axial velocity in the inviscid core remains independent of radius until one reaches the sidewall.

Lehmkuhl and Hudson [15] showed that shear layers can occur if both R_d/R_v and the axial gap H_v/R_v are sufficiently small. With respect to mass transfer, they demonstrated that effects from the side walls can be ignored if $R_d/R_v < 1/3$. These observations are in contrast to the bifurcation noted by Brady and Durlofsky [5] where it is observed that

https://doi.org/10.1017/S0956792515000145 Published online by Cambridge University Press

finite disk solutions have a collision region at $r = 0$ and are therefore not of similarity form for $r \to 0$ and that the outer edge of the disk excites unstable modes resulting in the a multitude of temporally unstable flows[7]. They qualify this statement by concluding that for moderate to high Reynolds number flows, the von Kármán similarity solution is useful as an approximation of the actual flow except possibly in the immediate vicinity of the axis of rotation. These observations are further supported for a small rotating upper disk, $R_d/R_v \ll 1$, in the work of Hyun and Kim [10] and the experimental results quoted therein. Some caution should be exercised due to the absolute instability of the flow discovered and confirmed experimentally by Lingwood [19, 20]. In light of these issues there is both experimental and theoretical evidence of flows within the apparatus having the general character of the classical von Kármán similarity solution.

Further details of the stability issue at $r = 0$ are elucidated in the review article by Zandbergen and Dijkstra [36] where the conflicting views of Stewartson [31] and Batchelor [2] with respect to rotating flow are detailed. Of particular interest is how Ockendon [26] was able to imply the existence of a whole family of solutions through the use of matched asymptotics to join inviscid solutions though viscous sublayers – a theme used by many subsequent papers to generate non-unique solutions.

References

[1] Abbad, M. & Chang, F. F. Schlumberger, Personal communication. The typical stone sample is 1.5 inches in diameter and held within a 5 inch diameter reaction vessel.
[2] Batchelor, G. K. (1951) Note on a class of solutions of the Navier–Stokes equations representing steady rotationally-symmetric flow. *Q. J. Mech. Appl. Math.* **4**(1), 29–41.
[3] Bernardez, L. A. (2008) Dissolution of polycyclic aromatic hydrocarbons from a non-aqueous phase liquid into a surfactant solution using a rotating disk apparatus. *Colloids Surf. A: Physicochemical Eng. Asp.* **320**(1), 175–182.
[4] Boomer, D. R., McCune, C. C. & Fogler, H. S. (1972) Rotating disk apparatus for reaction rate studies in corrosive liquid environments. *Rev. Sci. Instrum.* **43**(2), 225–229.
[5] Brady, J. F. & Durlofsky, L. (1987) On rotating disk flow. *J. Fluid Mech.* **175**(1), 363–394.
[6] Davies, C. W. (1962) *Ion Association*, Vol. 30, Butterworths, London.
[7] Escudier, M. P. (1984) Observations of the flow produced in a cylindrical container by a rotating endwall. *Exp. Fluids* **2**(4), 189–196.
[8] Fredd, C. N. & Fogler, H. S. (1998) The kinetics of calcite dissolution in acetic acid solutions. *Chem. Eng. Sci.* **53**(22), 3863–3874.
[9] Harned, H. S. & Hamer, W. J. (1933) The ionization constant of water and the dissociation of water in potassium chloride solutions from electromotive forces of cells without liquid junction. *J. Am. Chem. Soc.* **55**(6), 2194–2206.
[10] Hyun, J. M. & Kim, J. W. (1987) Flow driven by a shrouded spinning disk with axial suction and radial inflow. *Fluid Dyn. Res.* **2**(3), 175–182.
[11] Kaufmann, G. & Dreybrodt, W. (2007) Calcite dissolution kinetics in the system $CaCO_3$-H_2O-CO_2 at high undersaturation. *Geochim. Cosmochim. Acta* **71**(6), 1398–1410.
[12] Kern, D. M. (1960) The hydration of carbon dioxide. *J. Chem. Educ.* **37**(1), 14.
[13] Keslin, J. (1978) Viscosity of liquid water in the range −8 °C to 150 °C. *J. Phys. Chem. Ref. Data* **7**(3), 941–948.
[14] Lasaga, A. (1998) *Kinetic Theory in the Earth Sciences*, Princeton, New Jersey, Princeton University Press.

[7] Examples of some of the elaborate flow structures have been imaged in Escudier [7].

https://doi.org/10.1017/S0956792515000145 Published online by Cambridge University Press

[15] Lehmkuhl, G. D. & Hudson, J. L. (1971) Flow and mass transfer near an enclosed rotating disk: Experiment. *Chem. Eng. Sci.* **26**(10), 1601–1613.
[16] Lehto, P., Aaltonen, J., Niemelä, P., Rantanen, J., Hirvonen, J., Tanninen, V. P. & Peltonen, L. (2008) Simultaneous measurement of liquid-phase and solid-phase transformation kinetics in rotating disc and channel flow cell dissolution devices. *Int. J. Pharmaceutics* **363**(1–2), 66–72.
[17] Levich, V. G. & Spalding, D. B. (1962) *Physicochemical Hydrodynamics*, Vol. 689, Prentice-Hall, Englewood Cliffs, NJ.
[18] Lewis, G. N. & Randall, M. (1961) *Thermodynamics,* revised by K.S. Pitzer & L. Brewer, McGraw-Hill, New York.
[19] Lingwood, R. J. (1995) Absolute instability of the boundary layer on a rotating disk. *J. Fluid Mech.* **299**, 17–17.
[20] Lingwood, R. J. (1996) An experimental study of absolute instability of the rotating-disk boundary-layer flow. *J. Fluid Mech.* **314**(1), 373–405.
[21] Lund, K., Fogler, H. S. & McCune, C. C. (1973) Acidization–I. The dissolution of dolomite in hydrochloric acid. *Chem. Eng. Sci.* **28**(3), 691–700.
[22] Lund, K., Fogler, H. S., McCune, C. C. & Ault, J. W. (1975) Acidization–II. The dissolution of calcite in hydrochloric acid. *Chem. Eng. Sci.* **30**(8), 825–835.
[23] Miklavčič, M. & Wang, C. Y. (2004) The flow due to a rough rotating disk. *Z. für Angew. Math. Phys. (ZAMP)* **55**(2), 235–246.
[24] Mitchell, M. J., Jensen, O. E., Cliffe, K. A. & Maroto-Valer, M. M. (2010) A model of carbon dioxide dissolution and mineral carbonation kinetics. *Proc. R. Soc. A: Math. Phys. Eng. Sci.* **466**(2117), 1265–1290.
[25] Morse, J. W., Arvidson, R. S. & Lüttge, A. (2007) Calcium carbonate formation & dissolution. *Chem. Rev.* **107**(2), 342–381.
[26] Ockendon, H. (1972) An asymptotic solution for steady flow above an infinite rotating disc with suction. *Q. J. Mech. Appl. Math.* **25**(3), 291–301.
[27] Patnaik, P. (2003) *Handbook of Inorganic Chemicals*, Vol. 28, McGraw-Hill, New York.
[28] Pitzer, K. S. (1981) Characteristics of very concentrated aqueous solutions. *Phys. Chem. Earth* **13**, 249–272.
[29] Plummer L. N. & Busenberg, E. (1982) The solubilities of calcite, aragonite and vaterite in CO_2-H_2O solutions between 0 and 90 °C, and an evaluation of the aqueous model for the system $CaCO_3$-CO_2-H_2O. *Geochim. Cosmochim. Acta* **46**(6), 1011–1040.
[30] Prakongpan, S., Higuchi, W. I., Kwan, K. H. & Molokhia, A. M. (1976) Dissolution rate studies of cholesterol monohydrate in bile acid–lecithin solutions using the rotating-disk method. *J. Pharmaceutical Sci.* **65**(5), 685–689.
[31] Stewartson, K. (1953) On the flow between two rotating coaxial disks. *Proc. Camb. Philos. Soc.* **49**(2), 333–341.
[32] Taylor, K. & Nasr-El-Din, H. A. (2009) Measurement of acid reaction rates with the rotating disk apparatus. *J. Can. Pet. Technol.* **48**(6), 66–70.
[33] Tomlan, P. F. & Hudson, J. L. (1971) Flow near an enclosed rotating disk: Analysis. *Chem. Eng. Sci.* **26**(10), 1591–1600.
[34] Usdowski, E. (1982) Reactions and equilibria in the systems CO_2-H_2O and $CaCO_3$-CO_2-H_2O (0–50°C). *Neues Jahrbuch für Mineralogie. Abhandlungen* **144**(2), 148–171.
[35] Yuan-Hui, L. & Gregory, S. (1974) Diffusion of ions in sea water and in deep-sea sediments. *Geochim. Cosmochim. Acta* **38**(5), 703–714.
[36] Zandbergen, P. J. & Dijkstra, D. (1987) Von Kármán swirling flows. *Annu. Rev. Fluid Mech.* **19**(1), 465–491.
[37] Zeebe, R. E. (2011) On the molecular diffusion coefficients of dissolved CO_2, HCO_3^-, and CO_3^{2-} and their dependence on isotopic mass. *Geochim. Cosmochim. Acta* **75**, 2483–2498.

https://doi.org/10.1017/S0956792515000145 Published online by Cambridge University Press